Fine Tuning the Reactivity of Corrole-Based Catalytic Antioxidants

Zoya Okun and Zeev Gross*

Schulich Faculty of Chemistry, Technion-Israel Institute of Technology, Haifa 32000, Israel

ABSTRACT: In order to determine the electronic factors that may affect the catalytic antioxidant activity of water-soluble metallocorroles a series of 10-aryl-5,15-pyridinium manganese-(III) corroles was prepared. These complexes were examined regarding the effect of the C_{10} substituent on the Mn^{IV}/Mn^{III} redox potentials, catalytic rate constants for decomposition of HOONO, prevention of tyrosine nitration, and superoxide dismutase activity. This structure−activity relationship investigation provides new insight regarding the mechanism by which manganese(III) corroles act as catalytic antioxidants. It also discloses the superiority of the C_{10}-anysil-substituted complex in all examined aspects.

INTRODUCTION

Oxidative stress, the situation occurring due to an imperfect balance between the required and excessive amounts of reactive oxygen and nitrogen species (ROS and RNS), is nowadays well recognized as a key contributor to numerous diseases.[1] This may be exemplified by the diffusion-controlled coupling between superoxide and nitric oxide (both are free radicals of vital importance), whose combination leads to peroxynitrite (ONOO⁻) and subsequent transformation of its conjugated acid (HOONO, PN) into the most toxic ROS and RNS: •OH and •NO₂, respectively.[2−4] Both radicals are responsible for modifications of lipoproteins and cellular components, but nitration of tyrosine, cysteine, and tryptophan residues and subsequent inactivation of numerous vital enzymes that eventually may cause cell dysfunction and death is considered the main biomarker for involvement of PN.[5] The particularly severe cytotoxicity of PN may safely be attributed to the fact that there is no biological defense system against it, as all natural antioxidants (including diet-supplied and enzymes, such as superoxide dismutases and catalases) do not react with it faster than the vital biomolecules.[6]

A large variety of porphyrins and other strongly chelating ligands has been prepared for testing their potential regarding decomposition of ROS and RNS by the corresponding iron and manganese complexes.[7−12] The earliest synthetic antioxidants were developed as superoxide dismutase (SOD) mimics,[13] which may be attributed to the fact that involvement of PN and its decomposition products in biological systems was appreciated only much later.[14,15] Pioneering research on metalloporphyrins as SOD mimics was started by R. F. Pasternack in 1979 and continued by many others.[16] A particularly important contribution came from the Fridovich group, who established a structure−activity relationship (SAR) between the redox potential of manganese and iron porphyrins and their superoxide-dismutating activities in vitro and in vivo.[17] That research revealed that SOD activity increases when

the M(III)/M(II) redox potentials are anodically shifted, thus increasing the rate of $O_2^{-\bullet}$ oxidation by the chelated trivalent metal ions. Dramatic effects were achieved by introducing electron-withdrawing groups onto the β-pyrrolic positions of the porphyrin and imidazolium instead of pyridilium meso substituents.[18,19] The best-performing catalyst to date was reported by Batinic-Haberle's group: Mn(II)−β-octabromo-meso-tetrakis(N-methylpyridinium-3-yl)porphyrin, whose SOD-like activity approaches that of the enzyme itself.[20] Research regarding decomposition of PN by metalloporphyrins began in 1996 by M. K. Stern, who revealed that water-soluble iron(III) porphyrins function as "PN isomerases" by catalyzing the rapid isomerization of PN to nitrate.[21] This discovery was followed by intense research on manganese(III)-based water-soluble porphyrins by J. T. Groves and others, who realized that while the first step of PN reduction is very fast full catalysis is not achieved because of the slow reduction of the thus produced oxo−Mn(IV) intermediate back to the Mn(III) oxidation state.[22] Combination of Mn(III) porphyrin with biologically relevant reducing agents is, nevertheless, a powerful approach. While these naturally occurring antioxidants do not react fast enough with PN itself, they are very efficient for reducing oxo−Mn(IV) to Mn(III) and thus enable catalysis.[23]
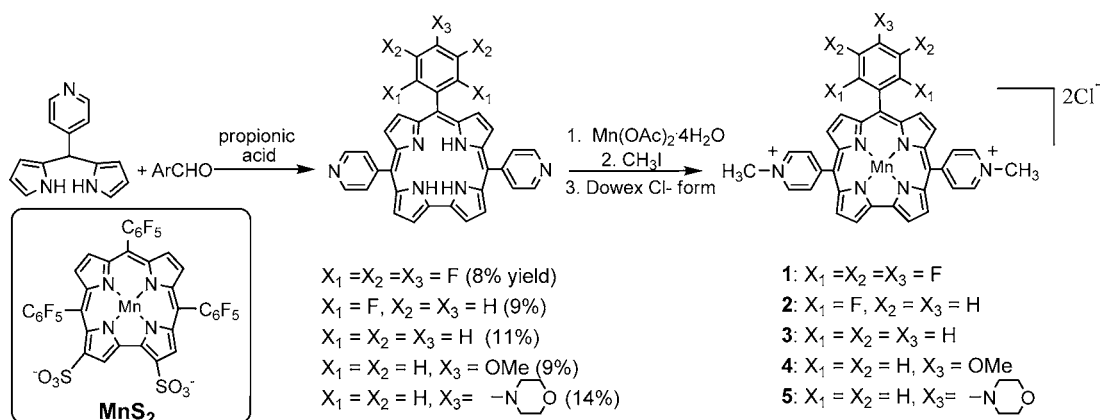
The most recently introduced catalytic antioxidants are based on water-soluble corroles, which have already been revealed to be highly potent for decomposition of PN,[24,25] superoxide radical,[26] and hydrogen peroxide.[27] The largest novelty of the iron(III) corroles is in their efficiency for H_2O_2 decomposition, which is not matched by other complexes (most are extensively bleached by it).[28] Manganese(III) corroles were identified as the first manganese complexes to display catalytic capability for PN decomposition in the absence of reducing agents as well as the only known catalyst for its disproportionation to benign
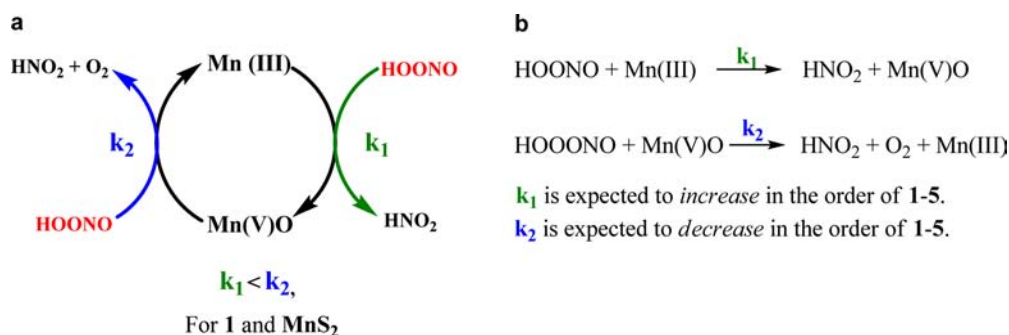
Scheme 1. Synthesis of Water-Soluble Corroles with Different C_{10} Aryls To Affect the Electron Richness of the Macrocycle and Chelated Manganese(III) Ion[a]

X$_1$ =X$_2$ =X$_3$ = F (8% yield)
X$_1$ = F, X$_2$ = X$_3$ = H (9%)
X$_1$ = X$_2$ = X$_3$ = H (11%)
X$_1$ = X$_2$ = H, X$_3$ = OMe (9%)
X$_1$ = X$_2$ = H, X$_3$= $-N\underset{\smile}{}O$ (14%)

1: X$_1$ =X$_2$ =X$_3$ = F
2: X$_1$ = F, X$_2$ = X$_3$ = H
3: X$_1$ = X$_2$ = X$_3$ = H
4: X$_1$ = X$_2$ = H, X$_3$ = OMe
5: X$_1$ = X$_2$ = H, X$_3$= $-N\underset{\smile}{}O$

[a]Inset: Structure of **MnS$_2$** with negatively charged head groups.

Scheme 2. Catalytic Cycle for PN Decomposition by Manganese(III) Corroles

a

b

$$HOONO + Mn(III) \xrightarrow{k_1} HNO_2 + Mn(V)O$$

$$HOOONO + Mn(V)O \xrightarrow{k_2} HNO_2 + O_2 + Mn(III)$$

k_1 is expected to *increase* in the order of **1-5**.
k_2 is expected to *decrease* in the order of **1-5**.

products.[24] These inventions were followed by studies on the cellular level for testing the metallocorrole's antioxidative properties in vitro. The results revealed cytoprotection by these catalysts on various cell lines used as models for diabetes,[29] atherosclerosis,[30,31] and neurodegenerative diseases,[32,33] including even some neurorescue effects. Importantly, the corrole complexes performed better than structurally related porphyrins in the examined applications. We now report on studies that focused on ways to increase the catalytic antioxidative performance of water-soluble manganese(III) corroles via establishment of a structure–activity relationship. Toward this goal we prepared a series of compounds similar to complex **1**, the most efficient manganese(III) corrole regarding catalytic decomposition of PN and superoxide radical. The new complexes, positively charged corroles that differ only in the C_{10} meso substituent, were examined regarding PN decomposition rates and prevention of nitration by it as well as for the ability to decompose superoxide radical. The results provide new insight regarding the mechanism by which manganese(III) corroles act as catalytic antioxidants. It also disclosed the superiority of the C_{10}-anysil-substituted complex in all examined aspects.

RESULTS AND DISCUSSION

A series of five corroles, with different C_{10} meso aryl substituents to affect electronic effects in a predictable fashion, was prepared using the synthetic route described in Scheme 1. Condensation of *para*-pyridyl-substituted dipyrromethane with aromatic aldehydes in refluxing propionic acid, without the aid of an oxidizing agent such as DDQ/*p*-chloranil (relying on air

as oxidant), yielded 8−14% of the desired compounds. The free-base corroles were characterized by NMR, UV−vis, and mass spectroscopies. Insertion of manganese was achieved by refluxing pyridine solutions of the corroles with manganese diacetate tetrahydrate, followed by alkylation with methyl iodide and I⁻/Cl⁻ ion exchange. This procedure led to the water-soluble manganese(III) corroles (**1−5**) bearing two positively charged substituents. This order of synthetic steps is better than alkylation before metalation, because the possible N-alkylation of the inner nitrogen atoms is avoided.[34] It is also easier to remove excess inorganic manganese salts before rather than after alkylation.

The motivation for preparing this particular series is based on previous research regarding PN decomposition by the negatively charged manganese(III) corrole **MnS$_2$** and the better performance of the positively charged **1**. One important observation was that attempts to follow photodiode array (PDA) spectral changes during PN decomposition by either **1** or **MnS$_2$** revealed no changes in the visible part of the spectrum during catalysis. This phenomenon and a variety of other indications were used to conclude that formation of (oxo)-manganese(V) corrole Mn(V)O is the rate-limiting step in the overall catalytic cycle (k_1, Scheme 2). We have now decided to investigate the effect of the corrole electron richness on the catalytic activity of the manganese complexes, based on the following hypothesis: Mn(III) will be more reducing when chelated by an electron-rich ligand, and as long as the Mn(V)O state will not be too stabilized, the overall catalytic constant for PN decomposition will increase. The predictions for each of the crucial steps in the catalytic cycle are outlined in Scheme 2b.
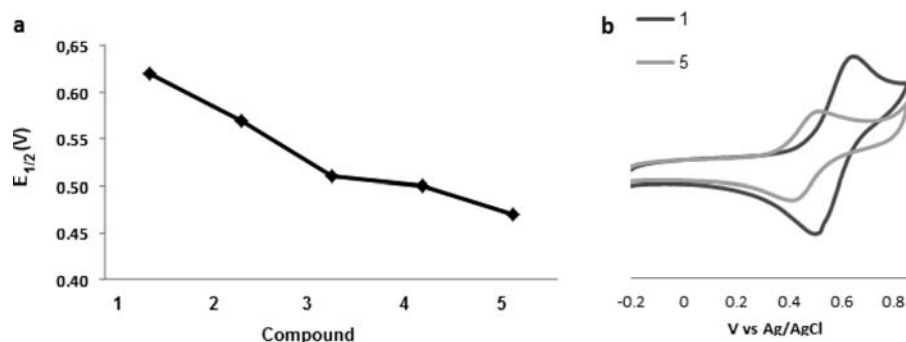
Figure 1. (a) Oxidation potentials (vs Ag/AgCl) of 0.8 mM **1−5** in acetonitrile with TBAP as electrolyte; scan rate 100 mV/s (the Fc/Fc$^+$ couple was 0.45 V under identical conditions), and (b) cyclic voltammograms of **1** and **5**.

Table 1. Oxidation Potentials (vs Ag/AgCl) of 1−5 in Acetonitrile with TBAP as electrolyte (the Fc/Fc$^+$ couple was measured as 0.45 V under identical conditions), PN Decomposition Rates, Amount of Nitrite Produced in the Decomposition Reaction, Attenuation of Tyrosine Nitration, and SOD Activity of the Examined Compounds

complex	$E_{1/2}$ (V) for Mn^{IV}/Mn^{III}	k_{cat} (10^5 M^{-1} s^{-1}) for PN decomposition	% of produced nitrite from PN	% of nitration attenuation 1 mM PN	% of nitration attenuation 2 mM PN	IC$_{50}$ (nm) for O$_2^{-\bullet}$ dismutation
1	0.62	1.58	62	42.3	39.1	181
2	0.57	1.67	64	45.2	42.2	160
3	0.51	2.0	68	55.1	51.6	25
4	0.50	2.73	92	57.3	53.1	20
5	0.47	1.82	76	56.3	48.6	26

An experimental evaluation of how the C$_{10}$ meso aryl substituents affect the electron richness of the chelated metal was obtained via examination of their Mn(IV)/Mn(III) redox couple. Cyclic voltammetry revealed that all manganese(III) corroles are oxidized at relatively low potentials to manganese-(IV) derivatives and that the redox potential gradually decreases from 0.62 V for the most electron-withdrawing **1** to 0.47 V for the most electron-releasing **5** (Figure 1 and Table 1). It may hence be concluded that the C$_{10}$ substituents stabilize the higher valent oxidation state increasingly more as a function of decreased electron-withdrawing ability. This in turn predicts that the manganese(III) corrole should become more reactive in the order of **1** to **5** (fastest acting) as long as k_1 of Scheme 2 is considered.

The rate by which the complexes decompose PN (5−20 μM catalyst, 400 μM PN, pH 7.4) was investigated by following the decay of PN at 302 nm using stopped flow kinetics. The second-order catalytic rate constants were deduced from the dependence of the pseudo-first-order rate constants on the catalyst's concentration (Figure 2, inset). A plot of the second-order rate constants versus the Mn(IV)/Mn(III) redox couples (Figure 2) reveals an increase from 1.6×10^5 M^{-1} s^{-1} for **1** to 2.7×10^5 M^{-1} s^{-1} for **4**. The larger potency for PN decomposition by **4** relative to **1−3** is consistent with the predicted effects of the C$_{10}$ substituents on k_1 of Scheme 2: the complexes with less electron-withdrawing aryls are more reducing, their k_1's are hence larger, and this effect on the rate-determining step is reflected in a larger k_{cat} in agreement with the proposed hypothesis. On the other hand, complex **5** does not fit within the above scenario, as its catalytic rate constant is lower than that of **4** and even **3**.

On the basis of the earlier introduced hypothesis (Scheme 2) the "anomaly" of **5** may be attributed to the increased stability of the Mn(V)O intermediate due to the highly electron-
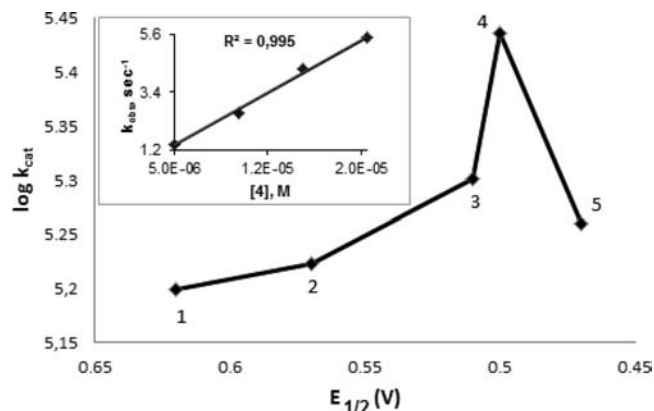

Figure 2. PN decomposition rates in aqueous pH 7.4 solutions catalyzed by the examined manganese(III) corroles in relation to their Mn(IV)/Mn(III) redox potentials (Inset) Plot used for determination of the catalytic rate constant of **4**.

donating p-morpholinophenyl group in **5**. Consequential reduction of k_2 may lead to a situation of $k_1 \approx k_2$ or $k_1 > k_2$, resulting in an overall smaller rate for decomposition of PN. Supporting evidence for this proposal was obtained from diode array spectra of catalytic PN decomposition by **5** and its comparison with the spectra of the manganese(III) corrole **5** and the independently prepared (via oxidation with iodosyl-benzene) (oxo)manganese(V) complex of the same corrole (**5-Mn(V)O**). As may be appreciated from Figure 3a, the main differences are as follows: (a) **5** has strong bands at 490 and 686 nm, absent for **5-Mn(V)O**; (b) the 420 nm band of **5-Mn(V)O** is much more pronounced than in **5**; (c) the 490/420 nm ratio of **5** is 1.4. In Figure 3b, the disappearance of PN (λ_{max} = 302 nm) is reflected in the spectral reduction at 280−350 nm and the 490/420 nm ratio is ~1:1. This suggests that the
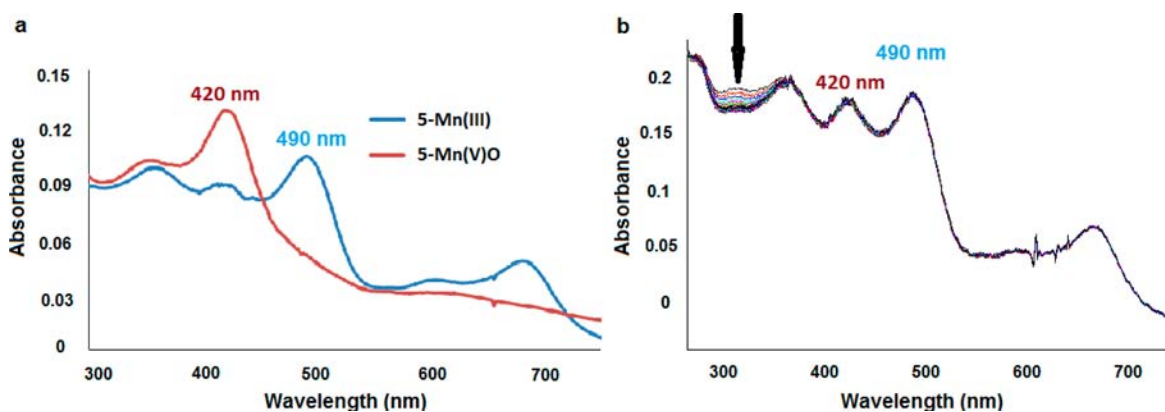
Figure 3. (a) Photodiode array spectra of PN decomposition by **5**, and (b) spectrum of independently prepared **5-Mn(V)O** from Mn(III), all in pH 7.4 phosphate buffer solutions.

"steady state" of the catalyst during catalysis is a mixture of Mn(III) (i.e., **5**) and Mn(V)O (i.e., **5-Mn(V)O**), consistent with a $k_1 \approx k_2$ situation. It is important to emphasize that this finding is unique of **5**: similar investigations on **1–4** revealed only Mn(III) during catalysis.

Previous research has revealed that manganese(III) corrole complexes decompose PN via disproportionation, yielding molecular oxygen and nitrite. Accordingly, we also examined the percentage of nitrite formation from PN (400 μM) via its decomposition in the presence of a fixed amount (10 μM) of the various catalysts. Spontaneous decay of PN is composed of homolytic bond cleavage and isomerization, both of which lead to nitrate and not nitrite. Accordingly, the $[NO_2^-]/[NO_3^-]$ ratio may be used for evaluating the competition between catalyzed and noncatalyzed reaction pathways. Nitrite concentration was quantified by the Griess reagent, which relies on development of a deep purple color (λ_{max} = 540 nm) whose intensity is directly correlated with nitrite concentration. The outcome of this investigation (Figure 4 and Table 1) resembled

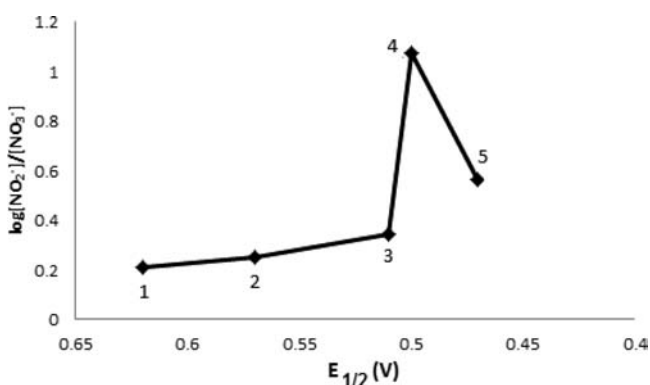**Figure 4.** Nitrite/nitrate ratio produced in the decomposition reaction of PN at 10 μM catalyst and 400 μM PN as a function of the Mn(IV)/Mn(III) redox potentials.

the results regarding the PN decomposition rate: the anysil-substituted complex **4** provided 92% nitrite, the more electron-poor catalysts provided less nitrite, and the most electron-rich **5** was less efficient than **4**.

The ability to prevent nitration of vital proteins and enzymes is one of the most desirable features required for potent catalytic antioxidants.[35] In this context, it is important to note that the main biomarker for involvement of PN is nitration of

aromatic amino acids.[36–39] In particular, excessive amounts of nitrotyrosine relative to healthy cells/tissues/organs are the first sign for a role of PN in numerous diseases.[40,41] On the basis of the above, the ability of complexes **1–5** to attenuate tyrosine nitration by PN was examined. Fixed concentrations of freshly prepared PN were added to 0.8 mM tyrosine solutions, with and without 50 μM of the complexes **1–5**, and incubated for 15 min at 37 °C. The amounts of unreacted tyrosine and produced 3-nitrotyrosine were quantified by HPLC analysis (Figure 5a), and the results for two different concentrations of PN are presented in Figure 5b and Table 1. The percentage of tyrosine nitration attenuation steadily increased from the most electron-withdrawing complex **1** to the anysil-substituted complex **4**, but the capability of **5** was lower than that of **4**.

To summarize the effects of the C_{10} aryls, determination of the Mn(III)/Mn(IV) redox potentials confirmed that increased electron richness leads to increased reducing power of the chelated manganese(III) in the order of **1** to **5**. It is however important to realize that changes in the electron-donating/withdrawing capabilities of the corrole macrocyclic could have conflicting effects on the fundamental steps of the overall catalytic cycle for decomposition of PN (Scheme 2). While k_1 might be anticipated to increase for more electron-rich manganese(III) corroles, k_2 should be affected in an opposite fashion. Since these rate constants are too fast to be determined independently, the evaluation is limited to the effect on the overall catalytic rate, k_{cat}. The results obtained by focus on three different phenomena show that electron-releasing aryls do increase k_{cat} as long as k_1 remains rate limiting. This situation changes in the most electron-rich complexes, for which decay of the stabilized (oxo)Mn(V) intermediate (k_2) is slower than its formation.

The improved insight into the mechanism of catalytic decomposition of PN raised our interest in investigating another recently reported activity of manganese(III) corroles: they catalyze also decomposition of superoxide radical.[26] PN decomposition and $O_2^{-\bullet}$ dismutation share similarities by virtue of one metal being responsible for both the reduction and the oxidation of the ROS. The difference is that PN decomposition by the manganese(III) corroles proceeds via two-electron processes (Scheme 2), while $O_2^{-\bullet}$ dismutation by the enzyme and all its synthetic mimics relies on one-electron redox reactions: oxidation and reduction of $O_2^{-\bullet}$, as depicted in eqs 1 and 2 (note that n = 3 for corroles but n = 2 for SOD and porphyrin-based SOD mimics), respectively. Accordingly, we
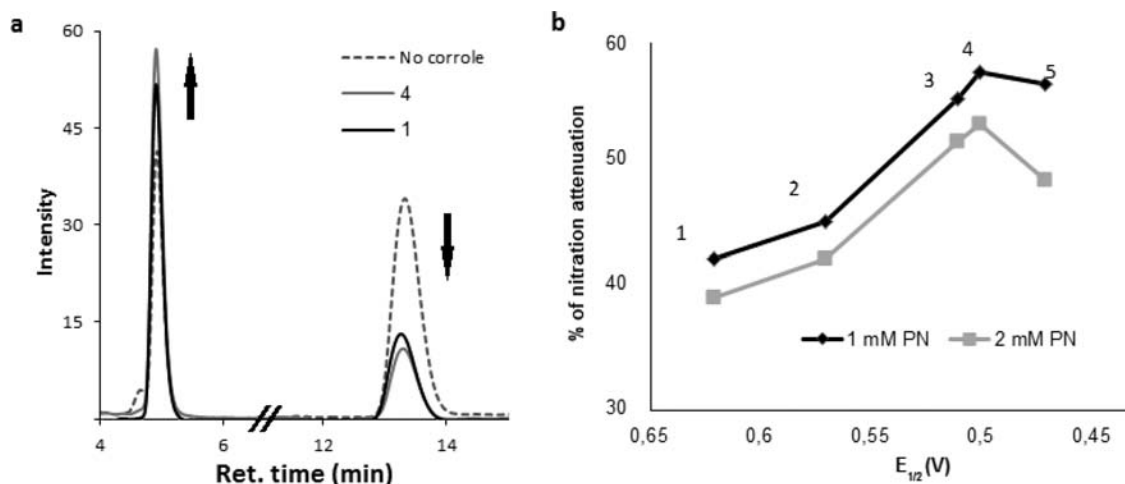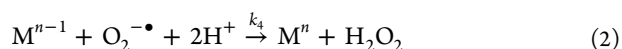
Figure 5. (a) Representative chromatograms used for evaluation of the ability of the manganese(III) corroles to prevent tyrosine nitration. (b) Attenuation of PN-induced tyrosine nitration by the examined compounds.

decided to examine the effect of the C_{10} aryls in **1−5** on the catalytic rates for $O_2^{-\bullet}$ dismutation thereby.

$$M^n + O_2^{-\bullet} \xrightarrow{k_3} M^{n-1} + O_2 \qquad (1)$$

$$M^{n-1} + O_2^{-\bullet} + 2H^+ \xrightarrow{k_4} M^n + H_2O_2 \qquad (2)$$

The well-known enzymatic assay, which is based on cytochrome *c* reduction attenuation,[42] was used for exploring the ability of **1−5** to decompose superoxide radical. To verify that the examined complexes do not inhibit production of superoxide by interaction with xanthine oxidase, we also monitored the formation rate of uric acid from xanthine with and without the examined compounds. Identical results were obtained by the two methods. Regarding the cytochrome *c* assay, very significant decreases in IC_{50} values were obtained as a function of the C_{10} aryl substituents: from 181 and 160 nM for the electron-poor **1** and **2** to 20 ± 3 nM for the more electron rich **3−5** (Figure 6 and Table 1).
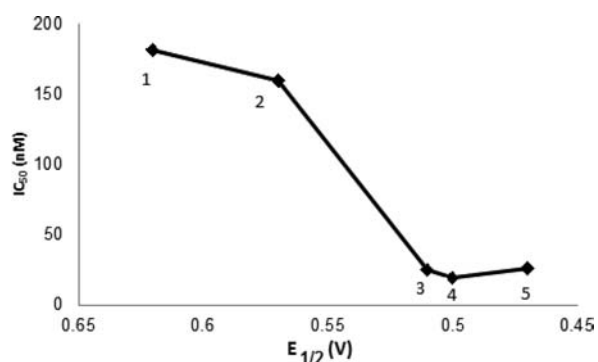

Figure 6. SOD activity of the examined manganese(III) complexes in relation to their Mn(IV)/Mn(III) redox potentials.

Analysis of these results with respect to eqs 1 and 2 suggests that (a) the rate-limiting step for **1** is k_3, (b) k_3 is increased in the order of **1** > **2** > **3−5**, (c) for **3−5** the rate-limiting step becomes k_4, and (d) the effect of the C_{10} aryls on k_4 is less pronounced than on k_3. Supporting evidence for these conclusions comes from the extensive knowledge of the correlation between metal redox potentials and SOD activity.[17]

With redox potentials of 0.47−0.62 V (vs Ag/AgCl), the only feasible reaction of the Mn(III) corroles with $O_2^{-\bullet}$ is that depicted in eq 2, i.e., transformation to Mn(IV). The thermodynamic driving force hence increases in the order of **1** > **2** > **3−5**. The predicted effect of the redox potentials on k_4 is in the opposite order, but the $E_{1/2}$ values of **3−5** are similar, which is the apparent reason for the similar catalytic rates that are obtained once k_4 becomes fully or partially rate limiting.

■ SUMMARY AND CONCLUSIONS

The main goal of the investigations was to obtain insight into the factors that determine catalytic antioxidant activity and to use the acquired mechanistic knowledge for design of catalysts with superior performance. We synthesized complexes **1−5**, five water-soluble manganese corroles that differ significantly in the electron-withdrawing capability of their C_{10} aryl substituent. Cyclic voltammetry revealed that the C_{10} substituents destabilize the manganese(III) oxidation state increasingly more as a function of decreased electron-withdrawing ability. This has been demonstrated to have a direct influence on the rate of PN decomposition, the percentage of PN disproportionation, attenuation of tyrosine nitration, and the effectiveness of superoxide radical dismutation. Evaluation of the overall order catalytic rate constants revealed a larger potency for PN decomposition by **4** relative to **1−3**, attributed to an effect on the first and rate-limiting step of catalysis. The most electron-donating C_{10} substituent present in complex **5** increased the stability of the Mn(V)O intermediate to an extent that led to a change in the rate-limiting step and a lower overall catalytic rate. Regarding tyrosine nitration, the most established biomarker for involvement of PN in diseases, the trend for PN decomposition fully came into account: the efficiency for preventing this reaction was in the order of **1** < **2** < **3** < **4** > **5**. Similar phenomena were seen in the examination of superoxide radical decomposition: the less electron-rich **1** and **2** displayed much larger IC_{50} values (lower efficiency) than the electron-poor **3−5**. Even though the elementary step in the catalytic decomposition of superoxide and peroxynitrite is significantly different, the similarity is that reduction by manganese(III) is the rate-limiting step for **1**. The rate of that elementary reaction and consequently the overall catalytic rate is increased for the more electron-rich complexes, but there is no more acceleration for **3−5** because the second step becomes rate limiting.

In summary, these structure–activity investigations have identified the anysil-substituted complex **4** as the best-performing manganese(III) corrole-based catalytic antioxidant regarding all examined aspects. We trust that the insight obtained in this work will be of great asset in the design of optimal catalysts for treating the many diseases that are affected by reactive oxygen and nitrogen species.

■ EXPERIMENTAL SECTION

Materials. The materials used for synthesis and workup procedures were purchased from Aldrich, Merck, Fluka, Riedel-de Haën, Biolab, and Frutarom and used as received unless otherwise stated. Deuterated solvents (Aldrich isotopes products) with a 99.5% minimum deuteration were used as received. Silica gel for column chromatography (Silica Gel 60, 63–200 μm mesh) was obtained from E. Merck Ltd. Most starting materials for syntheses were from Sigma-Aldrich and used without further purification. Pyrrole was run through a short basic alumina column, and aldehydes were purified by vacuum distillation before use. Tetrabutylammonium perchlorate as a supporting electrolyte in the CV experiments was obtained from Fluka and used after three recrystallizations from absolute ethanol. Electrodes for CV were obtained from CH Instruments.

Physical Methods. *Nuclear Magnetic Resonance Spectroscopy.* ^{1}H NMR and ^{19}F NMR spectra were recorded at room temperature on a Bruker Avance 400 III spectrometer equipped with automated tuning and matching on a broad band (BBFO) probe with gradients and 5 mm probe head. Chemical shifts are reported in ppm relative to residual hydrogen atoms of TMS ($\delta = 0.00$) or relative to CFCl$_3$ ($\delta_F = 0.00$).

Mass Spectrometry. Measurements were performed using a Micromass MS Technologies Maldi micro.

Cyclic Voltammetry. CV measurements were performed with a WaveNow USB potentiostat/galvanostat (Pine Research Instrumentation) using Pine AfterMath Data Organizer software. A three-electrode system consisting of a platinum wire working electrode, a platinum wire counter electrode, and an Ag/AgCl reference electrode was employed. CV measurements were performed using acetonitrile solutions of 0.3 M tetrabutylammonium perchlorate under nitrogen atmosphere at ambient temperature. The scan rate was 100 mV/s, and the $E_{1/2}$ value for the ferrocene/ferrocenium couple under these conditions was 0.45 V.

UV–Vis Absorption Spectroscopy. Absorption spectra were recorded with an Agilent 8453 diode array spectrophotometer.

Stopped-Flow Spectrophotometry. Fast kinetics experiments were performed on the AppliedPhotophysics RX.2000 rapid-mixing stopped-flow unit.

HPLC Analysis. Analyses were performed using a Merck Hitachi HPLC with a UV–vis detector system, equipped with a Luna 5u C18 Phenomenex column 250 × 4.6 mm, 5 μm. Commercially available tyrosine and 3-nitrotyrosine were used as standards.

Syntheses of Free-Base A$_2$B (A = pyridyl) Corroles: General Procedure. All of the examined compounds were synthesized by the previously developed method. In brief, aldehyde (42–76 mg, 0.4 mmol) was added to a 10 mL solution of 5-(4-pyridyl)dipyrromethane (178 mg, 0.8 mmol) in propionic acid, and the mixture was refluxed for 1 h. The residue obtained after solvent evaporation was washed with hot water, neutralized with ammonium hydroxide (25%), and washed again with hot water. Product purification and chemical yield are described for each compound.

5,15-Bis(pyridyl)-10-pentafluorophenylcorrole. This compound was prepared as previously published.[25]

5,15-Bis(pyridyl)-10-(2,6 difluorophenyl)corrole. Column chromatography: silica, hexane/EtOAc 1:1 followed by another column (silica, DCM/EtOH 150:1 and gradual increase of EtOH until 50:1. Fluorescent, dark-green-colored fractions afforded the desired corrole in 9% yield. All physical data recorded for the product was identical to that reported for the same compound obtained by a different synthetic route.[43]

5,15-Bispyridyl-10-phenylcorrole. Column chromatography: silica, hexane followed by gradual addition of EtOAc. Fluorescent, green fractions were released from the column at hexane/EtOAc 1:2. This was followed by crystallization (hexane/CH$_2$Cl$_2$ 2:1) to afford the desired corrole in 11% yield. UV–vis (CH$_2$Cl$_2$): λ_{max} ($\varepsilon \times 10^{-3}$) = 418 (30.4), 575 (3.4), 623 (2.4), 647 (2.3). MS (MALDI-TOF): m/z (%) 527 (100) [M$^+$]. ^{1}H NMR (400 MHz, C$_6$D$_6$), δ = 8.93 (unresolved doublet, 4H), 8.81 (d, J = 4.4 Hz, 2H), 8.73 (d, J = 3.6 Hz, 2H), 8.55 (unresolved doublet 2H), 8.37 (d, J = 6.8 Hz, 2H), 7.88 (unresolved doublet, 2H), 7.63 (t, J = 7.2 Hz, 4H), 7.53 (t, J = 7.2 Hz, 2H).

5,15-Bispyridyl-10-(4-methoxyphenyl)corrole. Column chromatography: silica, hexane/EtOac 1:1 followed by gradual increase of EtOAc until 100%, followed by another column (silica, DCM/EtOH 150:1 followed by a gradual increase of EtOH until 50:1). Collection of fluorescent dark-green-colored fractions afforded the desired corrole in 9% yield. UV–vis (CH$_2$Cl$_2$): λ_{max} ($\varepsilon \times 10^{-3}$) = 420 (48.9), 574 (6.6), 623 (4.8), 649 (4.7). MS (MALDI-TOF): m/z (%) 558 (100) [M$^+$]. ^{1}H NMR (400 MHz, C^{6}D^6): δ = 8.98 (d, J = 4.8 Hz, 4H), 8.80 (d, J = 3.6 Hz, 2H), 8.69 (d, J = 4.4 Hz, 2H), 8.64 (d, J = 4.4 Hz, 2H), 8.47 ppm (br s, 2H), 8.15 (d, J = 8 Hz, 2H), 8.02 (d, J = 5.2 Hz, 4H), 7.27 (d, J = 8 Hz, 2H), 3.60 (s, 3H).

5,15-Bispyridyl-10-(4-morpholinophenyl)corrole. Column chromatography: silica, EtOAc followed by crystallization (hexane/CH$_2$Cl$_2$ 1:1), affording the desired corrole in 14% yield. UV–vis (EtOAc): λ_{max} ($\varepsilon \times 10^{-3}$) = 421 (49.6), 577 (11.4), 620 (8.6). MS (MALDI-TOF): m/z (%) 613 (100) [M$^+$]. ^{1}H NMR (400 MHz, C$_6$D$_6$): δ = 8.96 (d, J = 5.0 Hz, 4H), 8.79 (d, J = 4.2 Hz, 2H), 8.77 (d, J = 4.7 Hz, 2H), 8.70 (d, J = 4.7 Hz, 2H), 8.45 ppm (d, J = 4.1 Hz, 2H), 8.24 (d, J = 8.3 Hz, 2H), 8.01 (d, J = 5.5 Hz, 4H), 7.12 (unresolved doublet), 3.71 (t, J = 4.6 Hz, 4H), 3.07 (t, J = 4.6 Hz, 4 H).

Manganese Insertion and Alkylation. Manganese insertion, alkylation, and ion exchange: free-base corrole 21–32 mg was refluxed in 5 mL of pyridine with 15 equiv of Mn(OAc)$_2$·4H$_2$O for 20 min, followed by chromatographic separation without solvent evaporation (dry silica, starting with CH$_2$Cl$_2$ and gradually adding methanol, unless otherwise stated). The product was dissolved in a minimal amount of hot THF, and excess methyl iodide 500 μL was added to the solution, which was then left at 40 °C until complete precipitation. Solid material was collected by centrifugation and washed with THF and diethyl ether until the solvent was colorless, affording pure **1−5**. The product was dissolved in a minimal amount of water, 500 mg of freshly HCl regenerated ion-exchange resin (Dowex 1:8 chloride form) was added, and the vessel was slowly shaken overnight. The resin was filtrated, and the solvent was lyophilized.

Manganese(III) 5,15-Bis(N-methylpyridinium)-10-pentafluorophenylcorrole (1). This compound was prepared as previously published.[25]

Manganese(III) 5,15-bis(N-methylpyridinium)-10-(2,6 difluorophenyl)corrole (2). Manganese insertion was performed as described by the general procedure starting with 21 mg of free base, affording 20 mg of the manganese(III) complex (89% yield). Product was dissolved in hot THF and alkylated as described by the general procedure, affording 27 mg of pure **2** (95% yield **2**). UV–vis (H$_2$O): λ_{max} ($\varepsilon \times 10^{-3}$) = 420 (13.2), 491 (28.0), 668 (9.7). MS (MALDI-TOF LD+): m/z (%) 646 (20) [M − 2Cl], 631 (100) [M − Me − 2Cl]. HRMS (m/z): [C$_{37}$H$_{25}$N$_6$F$_2$MnCl]$^+$ ([M − Cl]$^+$) calcd (found) 681.1178 (681.1177).

Manganese(III) 5,15-Bis(N-methylpyridinium)-10-phenylcorrole (3). Manganese insertion was performed as described by the general procedure starting with 29 mg of free base, affording 29 mg of the manganese(III) complex (91% yield). The product was dissolved in hot THF and alkylated as described by the general procedure, affording 39 mg of pure **3** (96% yield). UV–vis (H$_2$O): λ_{max} ($\varepsilon \times 10^{-3}$) = 355 (21.7), 424 (21.6), 490 (28.6), 680 (18.4). MS (MALDI-TOF LD+): m/z (%) 680 (10) [M], 645 (100) [M − Cl], 610 (10) [M − 2Cl], 580 (30) [M − 2Me − 2Cl]. HRMS (m/z): [C$_{37}$H$_{27}$N$_6$MnCl]$^+$ ([M − Cl]$^+$) calcd (found) 645.1366 (645.1347).

Manganese(III) 5,15-Bis(N-methylpyridinium)-10-(4-methoxyphenyl)corrole (4). Manganese insertion was performed as described by the general procedure starting with 28 mg of free base,

affording 27 mg of the manganese(III) complex (88% yield). Product was dissolved in hot THF and alkylated as described by the general procedure, affording 36 mg of pure **4** (94% yield). UV–vis (H_2O): λ_{max} ($\varepsilon \times 10^{-3}$) = 354 (15.9), 492 (32.1), 601 (8.54), 684 (16.3). MS (MALDI-TOF LD+) :m/z (%) 640 (100) [M − 2Cl], 625 (10) [M − Me − 2Cl], 610 (50) [M − 2Me − 2Cl]. HRMS (m/z): $[C_{38}H_{29}N_6OMnCl]^+$ ([M − Cl]$^+$) calcd (found) 675.1475 (645.1472).

Manganese(III) 5,15-Bis(N-methylpyridinium)-10-(4-morpholinophenyl)corrole (5). Manganese insertion was performed as described by the general procedure starting with 32 mg of free base, followed by chromatographic separation without solvent evaporation (dry silica, starting with EtOAc and gradually adding methanol), affording 29 mg of the manganese(III) complex (84% yield). Product was dissolved in THF and alkylated as described by the general procedure, affording 37 mg of pure **5** (91% yield). UV–vis (H_2O): λ_{max} ($\varepsilon \times 10^{-3}$) = 358 (12.2), 421 (11.8), 490 (14.6), 684 (6.7). MS (MALDI-TOF LD+): m/z (%) 695 (10) [M − 2Cl], 680 (100) [M − Me − 2Cl], 665 (20) [M − 2Me − 2Cl]. HRMS (m/z): $C_{41}H_{34}N_7OMn$ ([M − 2Cl]$^{2+}$) calcd (found) 695.2205 (695.2202).

PN Decomposition. PN was prepared according to a published procedure,[44] and the experimental procedures for studying its decomposition were identical to those reported in ref 25. Decomposition of 400 μM PN was measured with and without 5, 10, 15, and 20 μM of the examined compounds.

Nitrite Quantification. The amount of nitrite produced in PN decomposition experiments by different catalysts was quantified using the Griess reagent. A 15 μM concentration of the examined compound (dissolved in 0.3 M KH_2PO_4 pH 7 buffer) was reacted with 400 μM of freshly prepared PN (dissolved in 0.05 M NaOH). All samples were diluted by a factor of 10 before addition of the Grees reagent. Ninety-six well plates were used, and every reaction was examined in triplicate. A 50 μL amount of the sample was added to each well, followed by addition of 50 μL of sulfanilamide solution (1% sulfanilamide in 5% phosphoric acid) and incubation for 10 min (protected from light), 50 μL of 0.1% N-1-napthylethylenediamine dihydrochloride (NED) in water was added, and the plate was incubated in the dark for 10 min more. Absorbance at 540 nm was detected using a Spectramax M2Microplate Reader (Molecular Devices). Nitrite concentrations were determined relative to a standard curve. The background nitrite (from PN synthesis) was measured and subtracted from all samples by performing spontaneous decomposition of PN under acidic conditions (pH 3). As stated,[45−47] in acidic environment PN decomposes only via the isomerization mechanism, i.e., only nitrate is formed, so any measured nitrite originates from preparation of PN. Nitrite concentrations were determined relative to a standard curve.

Tyrosine Nitration. Tyrosine (0.8 mM) in 0.05 M phosphate buffer (pH 7.4) was reacted with either 1 or 2 mM PN with and without 50 μM of the examined compounds **1−5**. Samples were incubated at 37 °C for 15 min and kept on ice. The ability of **1−5** to inhibit PN-mediated reactions was expressed as the percentage of inhibition of 3-nitrotyrosine formation relative to the catalyst-free conditions. The amounts of tyrosine and nitrated tyrosine were determined by HPLC analysis.

The separation between tyrosine and 3-nitrotyrosine was achieved using a Luna 5u C18 Phenomenex column 250 × 4.6 mm. The mobile phase consisted of 0.05 M KH_2PO_4/H_3PO_4 (pH 3) and 10% methanol, the flow rate was 1 mL/min, and the detection wavelength was 275 nm. The injection volume of the samples was 40 μL. Tyrosine and 3-nitrotyrosine had a retention time of 5 and 13 min, respectively.

Cytochrome c Assay. Catalysis of dismutation of superoxide was measured using a xanthine oxidase/xanthine system as a source of superoxide and cytochrome c as the indicating scavenger of superoxide. Reduction of cytochrome c was followed at 550 nm. Assays were conducted at 25 ± 1 °C in 0.05 M phosphate buffer, pH 7.8 and 0.1 mM EDTA. IC_{50} values were determined by plotting $v_0/v_i − 1$ versus the concentration of corrole metal complex (v_0 is the rate of reduction of cytochrome c by superoxide and v_i is the rate of reduction of cytochrome c inhibited by corrole metal complex); IC_{50} is obtained when $v_0/v_i − 1 = 1$. Possible interference by inhibition of xanthine oxidase reaction by the examined compounds was ruled out following the rate of accumulation of urate at 290 nm in the absence of cytochrome c.

AUTHOR INFORMATION

Corresponding Author

*E-mail: chr10zg@tx.technion.ac.il.

Notes

The authors declare no competing financial interest.

REFERENCES

(1) Halliwell, B. G. J. *Free radicals in biology and medicine*, 4th ed.; Oxford University Press: New York, 2007.
(2) Goldstein, S.; Lind, J.; Merenyi, G. *Chem. Rev.* **2005**, *105*, 2457.
(3) Huie, R. E.; Padmaja, S. *Free Radical Res. Commun.* **1993**, *18*, 195.
(4) Beckman, J. S.; Koppenol, W. H. *Am. J. Physiol.* **1996**, *271*, C1424.
(5) Peluffo, G.; Radi, R. *Cardiovasc. Res.* **2007**, *75*, 291.
(6) Szabo, C.; Ischiropoulos, H.; Radi, R. *Nat. Rev. Drug Discovery* **2007**, *6*, 662.
(7) Rajic, Z.; Benov, L.; Kos, I.; Tovmasyan, A.; Batinic-Haberle, I. *Free Radical Biol. Med.* **2010**, *49*, S194.
(8) Rausaria, S.; Kamadulski, A.; Rath, N. P.; Bryant, L.; Chen, Z. M.; Salvemini, D.; Neumann, W. L. *J. Am. Chem. Soc.* **2011**, *133*, 4200.
(9) Spasojevic, I.; Batinic-Haberle, I.; Stevens, R. D.; Hambright, P.; Thorpe, A. N.; Grodkowski, J.; Neta, P.; Fridovich, I. *Inorg. Chem.* **2001**, *40*, 726.
(10) Day, B. J. *Drug Discovery Today* **2004**, *9*, 557.
(11) Radovits, T.; Seres, L.; Gero, D.; Lin, L. N.; Beller, C. J.; Chen, S. H.; Zotkina, J.; Berger, I.; Groves, J. T.; Szabo, C.; Szabo, G. *Mech. Ageing Dev.* **2007**, *128*, 173.
(12) Masini, E.; Cuzzocrea, S.; Mazzon, E.; Marzocca, C.; Mannaioni, P. F.; Salvemini, D. *Br. J. Pharmacol.* **2002**, *136*, 905.
(13) Batinic-Haberle, I.; Reboucas, J. S.; Spasojevic, I. *Antiox. Redox Signaling.* **2010**, *13*, 877.
(14) Ferrer-Sueta, G.; Radi, R. *Acs. Chem. Biol.* **2009**, *4*, 161.
(15) Blough, N. V.; Zafiriou, O. C. *Inorg. Chem.* **1985**, *24*, 3502.
(16) Pasternack, R. F.; Halliwell, B. *J. Am. Chem. Soc.* **1979**, *101*, 1026.
(17) Batinic-Haberle, I.; Spasojevic, I.; Hambright, P.; Benov, L.; Crumbliss, A. L.; Fridovich, I. *Inorg. Chem.* **1999**, *38*, 4011.
(18) Kachadourian, R.; Batinic-Haberle, I.; Fridovich, I. *Inorg. Chem.* **1999**, *38*, 391.
(19) Batinic-Haberle, I.; Spasojevic, I.; Stevens, R. D.; Hambright, P.; Neta, P.; Okada-Matsumoto, A.; Fridovich, I. *Dalton Trans.* **2004**, 1696.
(20) DeFreitas-Silva, G.; Reboucas, J. S.; Spasojevic, I.; Benov, L.; Idemori, Y. M.; Batinic-Haberle, I. *Arch. . Biochem. Biophys.* **2008**, *477*, 105.
(21) Stern, M. K.; Jensen, M. P.; Kramer, K. *J. Am. Chem. Soc.* **1996**, *118*, 8735.
(22) Lee, J. B.; Hunt, J. A.; Groves, J. T. *J. Am. Chem. Soc.* **1998**, *120*, 6053.
(23) Lee, J. B.; Hunt, J. A.; Groves, J. T. *Bioorg. Med. Chem. Lett.* **1997**, *7*, 2913.
(24) Mahammed, A.; Gross, Z. *Angew. Chem., Int. Ed.* **2006**, *45*, 6544.
(25) Gershman, Z.; Goldberg, I.; Gross, Z. *Angew. Chem., Int. Ed.* **2007**, *46*, 4320.
(26) Eckshtain, M.; Zilbermann, I.; Mahammed, A.; Saltsman, I.; Okun, Z.; Maimon, E.; Cohen, H.; Meyerstein, D.; Gross, Z. *Dalton Trans.* **2009**, 7879.
(27) Mahammed, A.; Gross, Z. *Chem. Commun.* **2010**, *46*, 7040.
(28) Mahammed, A.; Gross, Z. *Catal. Sci. Technol.* **2011**, *1*, 535.

(29) Okun, Z.; Kupershmidt, L.; Amit, T.; Mandel, S.; Bar-Am, O.; Youdim, M. B. H.; Gross, Z. *ACS Chem. Biol.* **2009**, *4*, 910.

(30) Haber, A.; Mahammed, A.; Fuhrman, B.; Volkova, N.; Coleman, R.; Hayek, T.; Aviram, M.; Gross, Z. *Angew. Chem., Int. Ed.* **2008**, *47*, 7896.

(31) Haber, A.; Aviram, M.; Gross, Z. *Chem. Sci.* **2011**, *2*, 295.

(32) Kupershmidt, L.; Okun, Z.; Amit, T.; Mandel, S.; Saltsman, I.; Mahammed, A.; Bar-Am, O.; Gross, Z.; Youdim, M. B. H. *J. Neurochem.* **2010**, *113*, 363.

(33) Kanamori, A.; Catrinescu, M. M.; Mahammed, A.; Gross, Z.; Levin, L. A. *J. Neurochem.* **2010**, *114*, 488.

(34) Gross, Z.; Galili, N. *Angew. Chem., Int. Ed.* **1999**, *38*, 2366.

(35) Szabo, C. *Br. J. Pharmacol.* **2009**, *156*, 713.

(36) Crow, J. P.; Ischiropoulos, H. *Nitric Oxide, Pt B* **1996**, *269*, 185.

(37) Peluffo, G.; Radi, R. *Cardiovasc. Res.* **2007**, *75*, 291.

(38) Radi, R. *Proc. Natl. Acad. Sci. U.S.A.* **2004**, *101*, 4003.

(39) Olmos, A.; Giner, R. M.; Manez, S. *Med. Res. Rev.* **2007**, *27*, 1.

(40) Pacher, P.; Beckman, J. S.; Liaudet, L. *Physiol. Rev.* **2007**, *87*, 315.

(41) MacMillan-Crow, L. A.; Crow, J. P.; Thompson, J. A. *Biochemistry* **1998**, *37*, 1613.

(42) McCord, J. M.; Fridovich, I. *J. Biol. Chem.* **1969**, *244*, 6049.

(43) Gryko, D. T.; Piechota, K. E. *J. Porphyrins Phthalocyanines* **2002**, 81.

(44) Hunt, J. A.; Lee, J.; Groves, J. T. *Chem. Biol.* **1997**, *4*, 845.

(45) Coddington, J. W.; Hurst, J. K.; Lymar, S. V. *J. Am. Chem. Soc.* **1999**, *121*, 2438.

(46) Edwards, J. O.; Plumb, R. C. *Prog. Inorg. Chem.* **1994**, *41*, 599.

(47) Lymar, S. V.; Hurst, J. K. *Inorg. Chem.* **1998**, *37*, 294.